SCIENTIFIC REPORTS

OPEN

Formation mechanism and optimization of highly luminescent N-doped graphene quantum dots

Dan Qu[1,3], Min Zheng[1], Ligong Zhang[1], Haifeng Zhao[1], Zhigang Xie[2], Xiabin Jing[2], Raid E. Haddad[4], Hongyou Fan[4,5] & Zaicheng Sun[1]

[1]State Key Laboratory of Luminescence and Applications, Changchun Institute of Optics, Fine Mechanics and Physics, Changchun 130033, Jilin, P. R. China, [2]State Key Laboratory of Polymer Physics and Chemistry, Changchun Institute of Applied Chemistry, Changchun 130022, Jilin, P. R. China, [3]University of Chinese Academy of Science, Beijing 100000, P. R. China, [4]Center for Micro-Engineering and Materials, Department of Chemical and Nuclear Engineering, University of New Mexico, Albuquerque, NM 87106, United State, [5]Sandia National Laboratories, Advanced Materials Laboratory, Albuquerque, NM 87106, United State.

Photoluminescent graphene quantum dots (GQDs) have received enormous attention because of their unique chemical, electronic and optical properties. Here a series of GQDs were synthesized under hydrothermal processes in order to investigate the formation process and optical properties of N-doped GQDs. Citric acid (CA) was used as a carbon precursor and self-assembled into sheet structure in a basic condition and formed N-free GQD graphite framework through intermolecular dehydrolysis reaction. N-doped GQDs were prepared using a series of N-containing bases such as urea. Detailed structural and property studies demonstrated the formation mechanism of N-doped GQDs for tunable optical emissions. Hydrothermal conditions promote formation of amide between $-NH_2$ and $-COOH$ with the presence of amine in the reaction. The intramoleculur dehydrolysis between neighbour amide and COOH groups led to formation of pyrrolic N in the graphene framework. Further, the pyrrolic N transformed to graphite N under hydrothermal conditions. N-doping results in a great improvement of PL quantum yield (QY) of GQDs. By optimized reaction conditions, the highest PL QY (94%) of N-doped GQDs was obtained using CA as a carbon source and ethylene diamine as a N source. The obtained N-doped GQDs exhibit an excitation-independent blue emission with single exponential lifetime decay.

Photoluminescent carbon or graphene quantum dots (GQDs) have received enormous attention because of their unique chemical, electronic and optical properties[1–4]. They also show good biocompatibility, low cytotoxicity, excellent water solubility and stable photoluminescence. These unique chemical and physical properties make them a great promising material for applications in photocatalyst, energy conversion, sensor, and bioimaging[5–17]. Various approaches have been developed to fabricate GQDs including "top–down" and "bottom–up" methods. The "top–down" methods refer to carving bulk carbon materials into nanoparticles by using physical or chemical approaches, such as acid oxidation[3,18], electrochemical[7,13], hydrothermal[11,19,20], etc. Compared with top-down routes, the bottom-up routes have obvious advantages in adjusting the composition and physical properties of GQDs by the careful selection of diversified organic precursors and carbonization conditions. Li and co-workers have made great effort to synthesize GQDs via stepwise solution chemistry based on oxidative condensation reactions[8,21]. Liu et al. prepared multicolor photoluminescent GQDs with uniform morphology by using hexa-peri-hexabenzocoronene as the carbon source through a pyrolysis and exfoliation process[12]. Loh et al. reported the synthesis of a series of well-defined GQDs on a ruthenium surface using C60 molecules as a precursor[22]. Besides the conjugated precursors used in above studies, some non-conjugate organic precursors have also shown great potential for the preparation of GQDs via thermal pyrolysis or carbonization. Tang et al. reported a facile microwave-assisted hydrothermal route for the synthesis of GQDs using glucose as the sole carbon source[23]. The size of GQDs can be tuned from 1.65 to 21 nm by simply prolonging the reaction time from 1 min to 9 min. The obtained GQDs showed size-independent photoluminescence (PL). Dong et al. prepared the blue luminescent GQDs through tuning the extent of carbonization of citric acid (CA)[24,25]. The resulting GQDs are nanosheets with 15 nm in width and 0.5–2.0 nm in thickness. The GQDs showed 9.0% of photoluminescent quantum yield (QY), and excitation-independent emission activity. Despite of previous efforts, the QY of GQDs has been relatively low. GQDs with high QY are highly desired for practical applications.
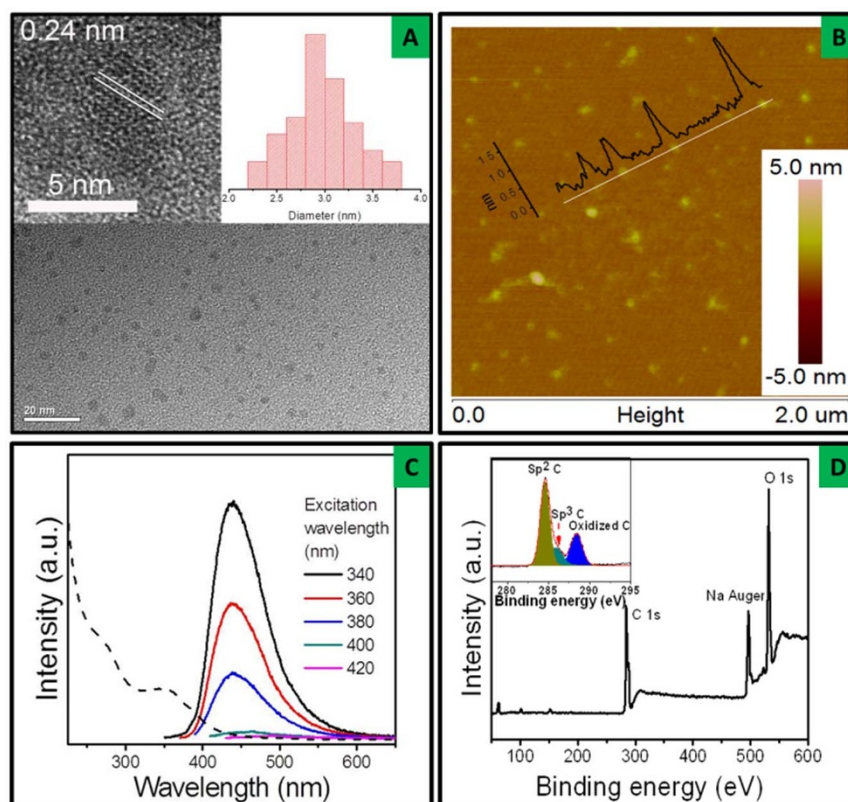
Figure 1 | Characterizations of GQDs-NaOH. (A) Representative TEM images of GQDs- NaOH. Inset panels show the HR-TEM image (left) and size (diameter) distribution (right). (B) SPM height image of the graphene nanoparticles. Line through some of the GQDs-NaOH shows the height profile. (C) UV-Vis spectrum (dash curve) and photoluminescence spectra (solid curves) of the graphene nanoparticles. (D) X-ray photoelectron spectroscopy (XPS) full scan survey and the high-resolution C1s spectra are shown in inset.

Doping and/or surface passivation are effective methods to change the electronic density of bulk semiconductor materials and to tune their optical and electrical properties. Through passivation and/or doping, GQDs have shown improved PL[3,26–30]. Herein, we synthesized N-doped GQDs and investigated the N-doping process of GQDs and their corresponding optical properties through a series of experiments. CA was used as the carbon source and different amines were used as the N source. We first synthesized GQD core materials by using NaOH as dopants. Under basic reaction condition, the CA molecules self-assembled into sheet structure followed by condensation reactions through intermolecular dehydroxylation, forming nanocrystalline GQDs. The final GQDs have unreacted functional groups such as carboxyl and hydroxyl groups on particle surface. At this point, the obtained GQDs show relative low QY of ~10%, excitation-independent PL, and single exponential lifetime. We then replaced NaOH with different amines to synthesize N-doped GQDs. We discovered that N atom enters GQDs by forming pyrrolic structure through intramolecular dehydroxylation between neighbor carboxyl groups. Pyrrolic N is gradually transferred into quaternary N in the graphene with increasing the reaction time. The extent of doping effectively improves the optical properties of GQDs, especially QY of N-doped GQDs. We investigated the influence of the types of amines, such as primary, secondary and ternary amines. The primary amine resulted in a high doping degree and the N-doped exhibited the highest QY among the three types of amines. When ethylene diamine (EDA) was used as the dopant, N-doped GQDs showed a QY of 94%, which is the highest QY reported to our knowledge. Besides the investigation on three types of amines, we also optimized the reaction conditions of CA and EDA reaction including carbon sources, reaction time, and reaction temperature in order to obtain high PL QY of the N-doped GQDs. Overall, the resulted GQDs showed excitation independent and single exponential decay.

Results

Formation of graphene core materials using NaOH (GQDs-NaOH). No GQDs were formed when pure CA was used in hydrothermal reactions without using bases (*e.g.*, NaOH, amines). NaOH was added as a base into the reaction solutions followed by adjusting the solution pH to 8. After hydrothermal reaction, a light yellow solution with blue emission under UV light was obtained, which is the same as the GQDs prepared from sodium citrate. Transmission electron microscopy (TEM) images of the resulting GQDs-NaOH (Figure 1A) show that these GQDs are uniform in size ranging from 1.8 to 3.8 nm in diameter. High resolution TEM (HR-TEM) (Figure 1A inset) clearly shows the lattice fringes measured to be 0.24 nm, which corresponds to the (1120) crystal phase of graphite[18,31]. Some GQDs particles also showed the lattice fringe of 0.35 nm, which attributes to the (002) crystal phase of graphite. Scanning probe microscopy (SPM) images (Figure 1B) further confirm the uniformity of the GQDs. The SPM height profile in Fig 1B inset revealed that a typical topographic height of the GQDs ranges from 0.5 to 2.0 nm. This suggests that these GQDs consist of 1–5 graphene layers. As shown in the UV-Vis spectrum in Figure 1C, the GQDs show two absorption bands at 270 nm and 350 nm. A strong blue emission at 450 nm was observed under excitation of 340 nm–400 nm. This photoluminescent emission band did not shift with the change of excitation wavelength. The calculated QY is ~22%. X-ray photoelectron spectroscopy (XPS) measurement was performed to determine the GQD composition. The full scan XPS spectrum of GQDs-NaOH was shown in Figure 1D. C1s, Na auger and O1s signals were observed at 284,
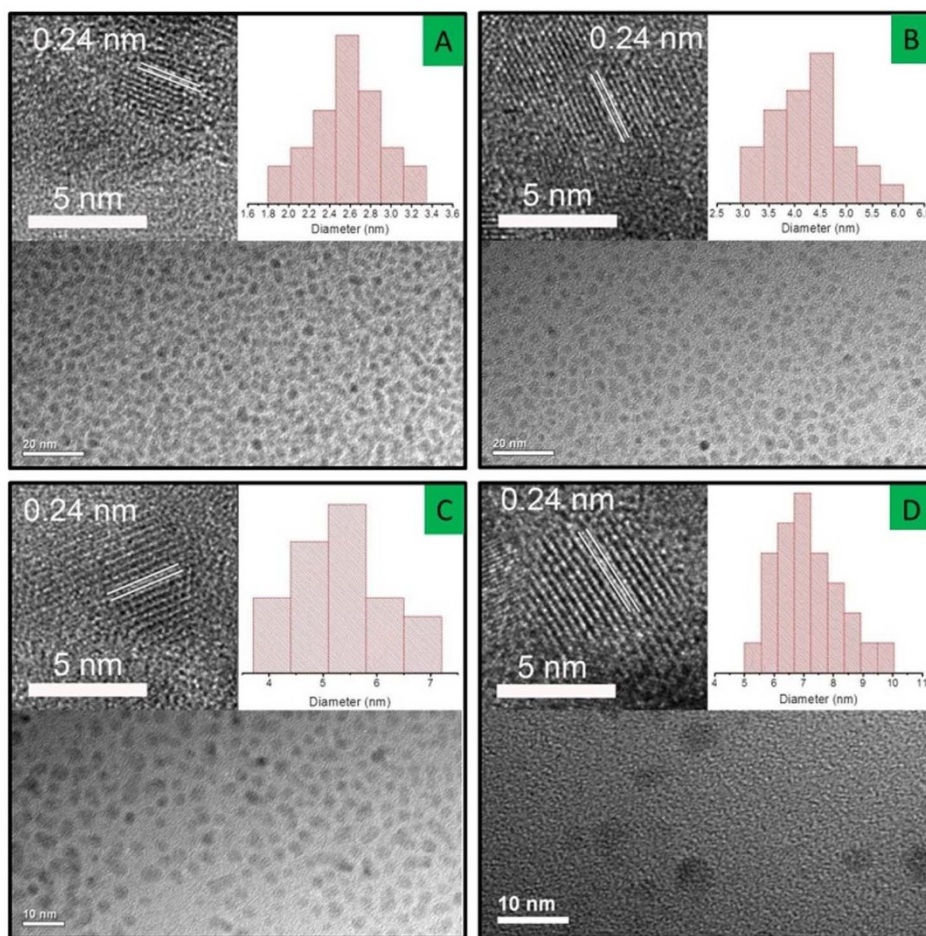
Figure 2 | Representative TEM images of GQDs-U samples prepared at (A) 4 hours, (B) 6 hours, 8 hours, and (C) 24 hours. The corresponding HR-TEM images and particle size distribution are shown as left and right insets, respectively.

399 and 530 eV, respectively. No N peak was observed in full scan XPS survey. That confirms GQDs-NaOH does not contain N element. The element analysis result also showed no N element was detected. These results disclose that the as-obtained GQDs-NaOH are N free GQDs in this case. The high-resolution C1s XPS spectrum can be fitted into three Gaussian peaks at 284.5, 285.9, and 288.4 eV, which attribute to sp^2 C (C-C, C=C), sp^3 C (C-O) and oxidized C (C=O), respectively. Based on above results, we can conclude that the GQDs were formed through dehydrolysis process between CA molecules that is promoted by the weak basic environment due to the formation of citrate salt.

N-doping processes of GQDs using urea (GQDs-U). To prepare high luminescent N-doped GQDs, urea was chosen because it could be used as both a base and the N source for N-doping processes. A series of samples were prepared at different reaction time (samples are denoted as GQDs-U-n, n is reaction time). Figure 2 and Supplementary Figure S1 showed the TEM images of GQDs-U-n samples at different reaction times from 2 to 24 hours. The overall size of GQDs–U increases as the reaction time increases. The average sizes of GQDs-U-n are 2.45 ± 0.26, 2.58 ± 0.34, 4.3 ± 0.7, 5.26 ± 0.78 and 7.11 ± 1.06 nm in diameter for the samples prepared at from 2, 4, 6, 8 and 24 hours, respectively. The related HR-TEM images showed that all the GQDs-U exhibited highly crystalline graphite nature. The measured lattice fringe distance is 0.24 nm, which corresponds to the (1120) crystal phase of graphite. The UV-Vis and PL spectra are showed in Supplementary Figure S1 and S2 in Supplementary Information. There are two clear absorption bands at 234 nm and 340 nm, which is close to

previous reports[32]. These absorption bands are related to $\pi \rightarrow \pi^*$ and $n \rightarrow \pi^*$ transition of C=C and C=O bond in the GQDs. All GQDs-U samples show excitation-independent and narrow photoluminescent emission band at 450 nm and full width at half maximum is ~65 nm, which suggests both the size and the surface state of these GQDs should be uniform[24]. Besides, the lifetimes (τ, Supplementary Figure S1, S3) of GQDs-U samples are 8 ns, which is single exponential decay. This suggests that the origin of PL is one single species.

Figure 3 and Supplementary Figure S1B showed the XPS results of GQDs-U-n samples. N signal can be barely seen in the GQDs-U-2 sample. In high-resolution N1s XPS of GQDs-U-2, there is a weak N 1s signal at 400.0 eV, which is close to the pyrrolic N. These results indicate that the graphene framework has formed at this stage, but only trace amount of N can enter the graphene framework. In full scan XPS spectra of GQDs-U-4~24 (column A in Figure 3), the N peak intensity turned stronger and stronger with extended reaction time. The peak intensity ratios of N1s/C1s ($R_{N/C}$) were calculated from full survey XPS spectra. The $R_{N/C}$ increased from 0.22 to 0.48 (Supplementary Figure S4). This indicates that N doping degree of GQDs increases with reaction time. The high-resolution C1s XPS spectra were shown in column B of Figure 3. The spectra can be fitted into 3 Gaussian peaks at 284.5, 286.1, 288.6 eV, which correspond to the sp^2 carbon (C-C/C=C) in graphene, the sp^3 carbon (C-O and C-N), and the C=O in carboxyl group. The relative intensity ratio of sp^3 and sp^2 increases with the increasing of reaction time because more N atoms enter the graphene structure. High-resolution N1s XPS spectra were shown in column C of Figure 3. The high-resolution N1s XPS peak of GQDs-U-2 appeared at 400 eV, which contributed from
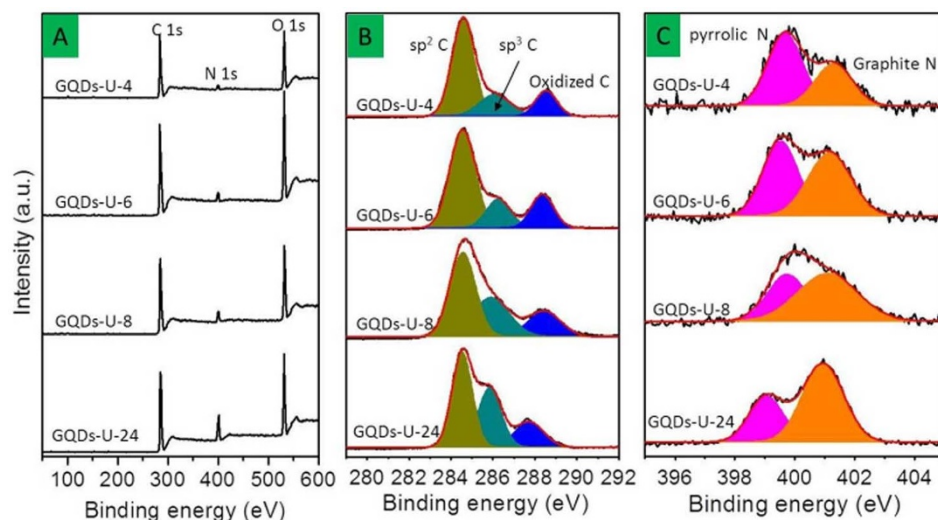
Figure 3 | XPS spectra of GQDs-U-4, GQDs-U-6, GQDs-U-8 and GQDs-U-24. Column A is the full scan survey, column B is the high-resolution C1s XPS spectra, and column C is the high-resolution N1s XPS spectra.

the pyrrolic N. The spectrum can be fitted with 2 Gaussian peaks at 399.8 and 401.5 eV that correspond to the pyrrolic N and graphite N, respectively[25,33]. Existence of Pyrrolic N indicates that N bonds with C in 5 member-ring structures that are formed from dehydrolysis between the neighbor carboxyl and amide groups (Figure 4). Graphite N originates from the N atoms that are bonded with 3 neighbor C atoms. With the increase of reaction time, more and more N atoms enter the graphene layer, which leads to the increase

of the sp³ C. This is consistent with the fact that the relative amount of graphite N in the GQDs-U increases with the reaction time. Element analysis results also show the same trend that the amount of N increases with the reaction time (Supplementary Table S1), indicating that the extent of N-doping increases with the reaction time. Supplementary Figure S5 showed the FTIR spectra of N-doped GQDs-U prepared at different reaction time. There is a shoulder peak at 1712 cm⁻¹ that can be assigned to the carboxyl acid groups
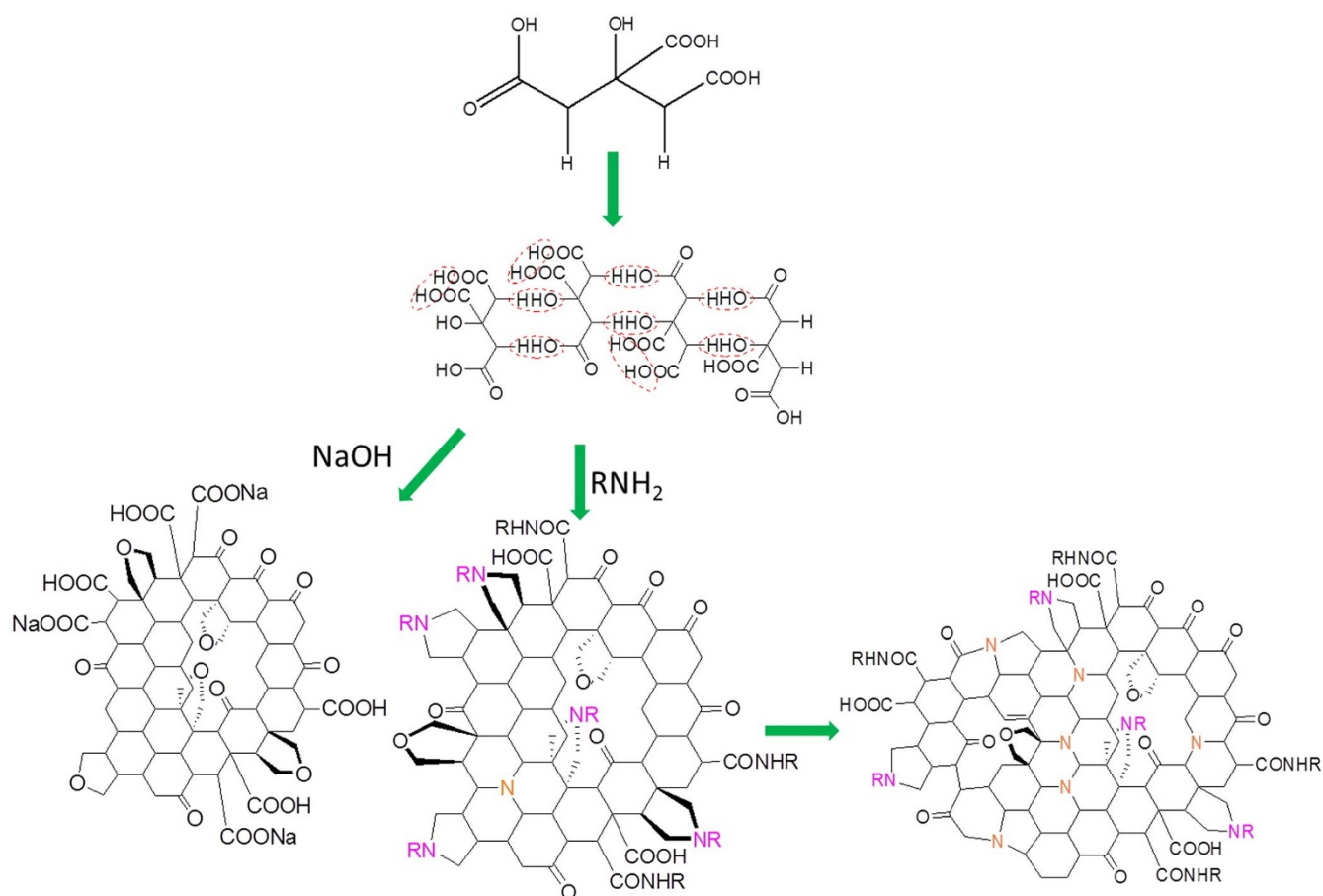

Figure 4 | Possible formation process of N-doped GQDs.

Table 1 | PL QY and life time of all GQDs samples

Sample	PL QY (%)	τ_{ave} (ns)
GQDs-NaOH	22	7
GQDs-U-2	58	8
GQDs-U-4	78	8
GQDs-U-6	80	8
GQDs-U-8	81	8
GQDs-U-24	82	8
GQDs-HMTA	20	10
GQDs-DEA	30	7
GQDs-EA	36	6
GQDs-EDA	94	14
GQDs-G	6	7
GQDs-TRIS	16	6

τ_{ave}: average lifetime.

(-COOH). Along with the reaction, this peak disappears, suggesting the consumption of –COOH groups due to the dehydrolysis. In addition, two new shoulder peaks at 1700 and 1642 cm^{-1} gradually show up with the increase of reaction time. These new peaks contribute to formation of amide in the N-doped GQDs. The absolute PL QY increases from 58% to 81% with increasing reaction time from 2 to 24 hours (Table 1).

The influence of the types of amines on QY. GQDs were synthesized using different kinds of amine such as tertiary, secondary, and primary amine (mono and diamine) in order to investigate the effect of the types of amines. The GQDs-HMTA, GQDs-DEA, GQDs-EA and GQDs-EDA are used to denote the GQDs that were prepared using hexamethylene tetraamine (HMTA), diethylene amine (DEA), ethanol amine (EA), and ethylene diamine (EDA), respectively. Figure 5A–C showed TEM images of GQDs-HMTA, GQDs-DEA, and GQDs-EA. TEM images showed these three GQDs are monodispersed with a
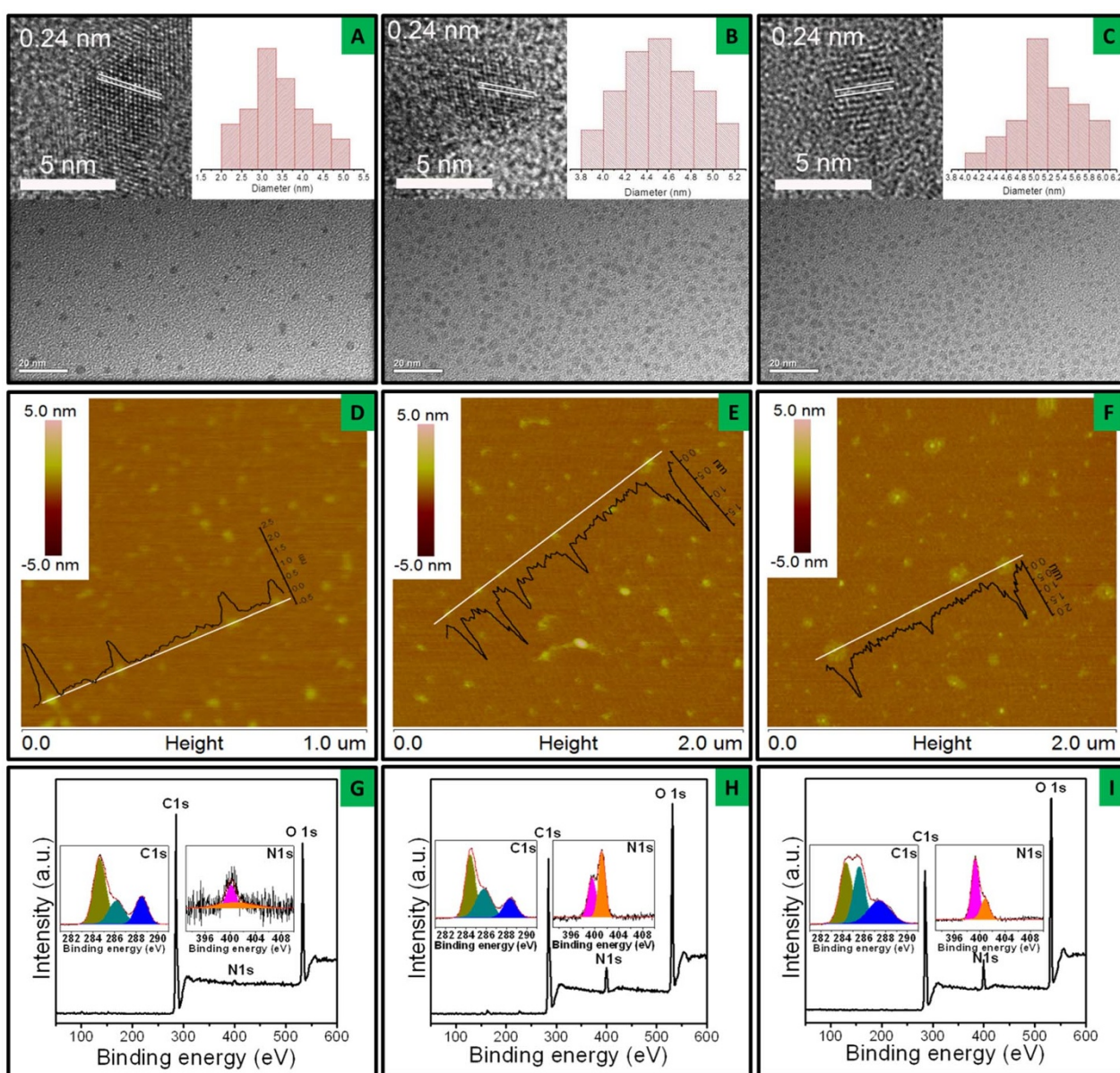

Figure 5 | Representative TEM images (A–C), SPM images (D–F) and XPS spectra (G–I) of GQDs-HMTA, GQDs-DEA and GQDs-EA. Left and right insets are the corresponding HR-TEM images and particles size distribution in A–C. The height profiles in D–F are inserted along the line cut. High resolution C 1s and N1s spectra are inserted in the full scan survey in G–I.
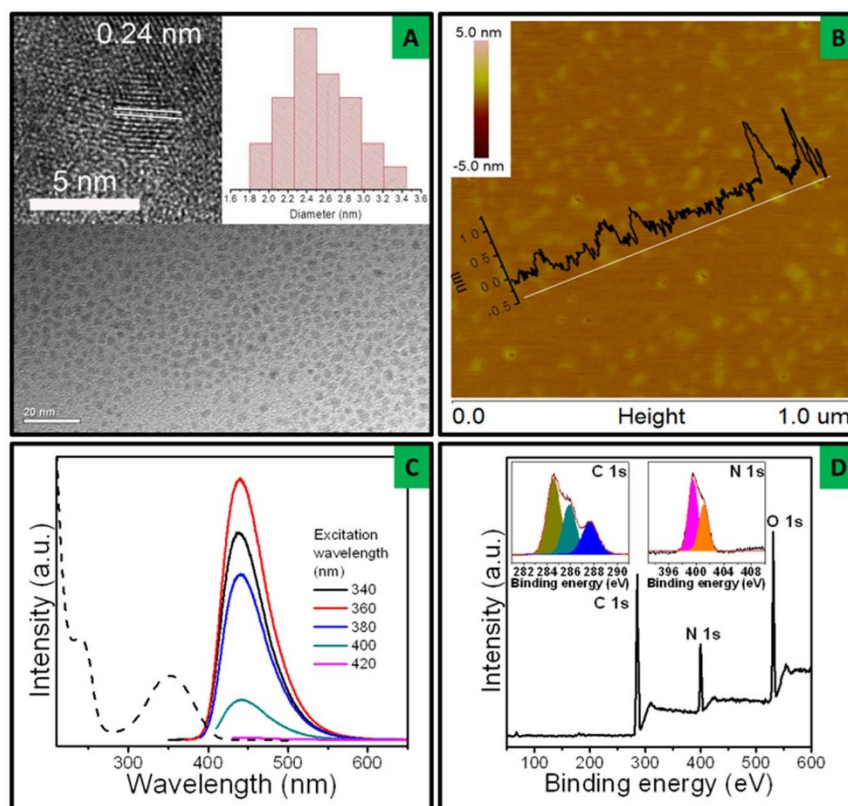
Figure 6 | Characterizations of GQDs-EDA. (A) Representative TEM images of GQDs-EDA. Insets: HR-TEM image (left) and particles size (diameter) distribution (right). (B) SPM height image of GQDs-EDA. (C) UV-Vis spectrum (black dash curve) and photoluminescence spectra. (D) XPS full scan survey. Inset: high-resolution C 1s and N1s XPS spectra.

uniform diameter of 3.39 ± 0.69 nm, 4.53 ± 0.27 nm, 5.13 ± 0.47 nm, respectively. HR-TEM images confirmed that GQDs-HMTA showed a lattice fringe with 0.24 nm, which corresponds to the (1120) crystal phase of graphite. The corresponding SPM height image revealed a typical topographic height of 1–2.0 nm (Figure 5D–E), indicating that most of the GQDs consist of ca. 1–5 graphene layers[12,31]. Raman spectrum (Supplementary Figure S6) was employed to further characterize the microstructure of GQDs-HMTA. GQDs-HMTA shows a disordered (D) band at 1359 cm^{-1}, related to the presence of sp^3 defects, and the crystalline (G) band at 1578 cm^{-1}, related to in-plane vibration of sp^2 carbon. The ratio of the intensities (I_D/I_G) of these characteristic bands can be used to correlate the structural properties of the carbon. The value of I_D/I_G is 0.9 for GQDs-HMTA, meaning that the as-prepared GQDs-HMTA have highly crystalline nature, which is consistence with the TEM results. The optical properties of GQDs-HMTA, GQDs-DEA and GQDs-EA are shown in Supplementary Figure S7. All GQDs exhibit a shoulder band at 235 nm and a clear absorption band ~340 nm, which is close to GQDs-U. The PL spectra show all GQDs have an emission at 450 nm that is excitation-independent. This further suggests that both the size and the surface state of these GQDs are uniform. The measured lifetime of GQDs-HMTA, -DEA, and -EA are 10, 7 and 6 ns, respectively, showing single exponential decay (Supplementary Figure S8).

Although these three GQDs samples have close structures and similar optical properties, they have different PL QY of 20%, 30% and 36% for GQDs-HMTA, GQDs-DEA and GQDs-EA, respectively. From XPS studies of these GQDs, we found that the QY differences might be caused by the different extent of N-doping within these three samples. The full scan XPS spectra of GQDs-HMTA, GQDs-DEA, and GQDs-EA are shown in Figure 5G–I. The full scan XPS of GQDs-HMTA shows a predominant C 1s peak at 284 eV and

O 1s peak at ~532 eV. No significant N 1s peak at 401 eV was observed for GQDs-HMTA. Even high-resolution N 1s spectrum also shows a relative weak signal. Element analysis results show that the GQDs-HMTA contains C 43.62%, H 6.28% and N 0.89%, suggesting the trace amount of N. Evidences from FTIR spectrum of GQDs-HMTA (Supplementary Figure S9) further confirm this. The peak at 1714 cm^{-1} is attributed to the vibration of C=O in -COOH. There is no peak appear at ~1670 cm^{-1}, which indicates there exists no amide group in the GQDs-HMTA sample. The XPS, element analysis, and FTIR results indicate the GQDs-HMTA is also N free GQDs like GQDs-NaOH. Comparing with that of GQDs-HMTA, XPS results of GQDs-DEA and GQDs-EA exhibit relatively high N amount in the samples. The $R_{N/C}$ of GQDs-DEA and GQDs-EA are 0.31 and 0.37. It obviously primary amine have highest doping degree among three types amine. The PL QY was improved from 20% to 30% and 36% for the samples of GQDs-DEA and EA, respectively. Based on the XPS results, primary amine is the best dopant for the N doped GQDs among these three types of amines.

Although the PL QY of GQDs-EA show the highest PL QY among the primary, secondary and tertiary amine, the GQDs-U series samples show much higher PL QY comparing with the GQDs-EA. We increased the amount of EA, no significant improvement of PL QY was obtained. (Supplementary Table 1) Since urea could be treated as a diamine that gives us a hint that diamine may be a better dopant than monoamine. Then we chose ethylene diamine (EDA) as a dopant for preparing N doped GQDs. TEM images of GQDs-EDA, as shown in Figure 6A, reveal that the GQDs-EDA are uniform and have a diameter of 2.30 ± 0.31 nm. The HR-TEM images exhibit clear lattice fringe of 0.24 nm, which discloses that the GQDs-EDA also have a graphite nature. AFM image of GQDs-EDA (Figure 6B) discloses the sheet structure, which is about ~1 nm in thickness. UV-Vis spectrum of GQDs-EDA exhibits 2 clear absorption bands

Table 2 | PL QY of GQDs-EDA prepared at different reaction conditions

Sample	1 h	4 h	8 h	24 h
140°C	68	79	72	65
160°C	88	94	90	76
180°C	77	82	78	69
200°C	65	76	72	61

at 235 and 340 nm, which are the same as GQDs-U. A strong and bright blue emission at 450 nm that is excitation-independent emission, was observed in the PL spectrum. GQDs-EDA exhibits a much longer lifetime of 14 ns that is almost double longer than GQDs-U. The full scan XPS spectrum (Figure 6D) shows three signals at 284, 399 and 521 eV that are attributed to C 1s, N1s, and O1s respectively. The $R_{N/C}$ is 0.59, which is higher than any other N doped GQDs in this report. High-resolution C 1s spectrum revealed that there exist three types of C including sp^2 C (C=C), sp^3 C (C-C, C-N, and C-O), and oxidized C (C=O). Two types of N, pyrrolic N and graphite N are shown in the high-resolution N 1s spectrum. These results indicate that the extent of doping of GQDs-EDA increases from monoamine to diamine. Due to the higher doping degree, the PL QY of GQDs-EDA also exhibits very high PL QY of 94%, which is the highest PL QY of GQDs to our knowledge. Comparing with GQDs, N doping introduces a new surface state labeled as the N-state[25,34]. Electrons trapped by the N-state are able to facilitate a high yield of radiative recombination and depress non-radiative recombination. The density of N-state strongly affects the PL QY of GQDs. The higher N doping degree is in GQDs, the higher density of N-state

is. From above results, the N doped GQDs are hardly obtained from tertiary amine as dopant because it has no active N-H. As a dopant, primary amine is better than secondary amine; diamine is a better dopant than monoamine.

The influence of reaction time and temperature on QY. We optimized the reaction conditions such as reaction temperature, reaction time, and the ratio of reactant for preparation of high quality GQDs using CA and EDA. Table 2 shows the PL QY of N-doped GQDs obtained from CA and EDA under different reaction conditions. The reaction temperature and time show a parabolic trend. The optimum reaction temperature and time are 160°C and 4 hours, respectively. The molar ratio of CA and EDA was changed from 1:1 to 1:7, the PL QY of all the GQDs are above 80% (Supplementary Table S2). The optimum ratio of CA and EDA is 1:3, the PL QY of GQDs reaches 94%.

The influence of carbon source on the PL QY. We synthesized GQDs using other carbon sources such as glucose and TRIS under the same hydrothermal route. Figure 7 shows the TEM images of GQDs prepared from glucose (GQDs-G) and TRIS (GQDs-TRIS) as carbon source. The graphite lattice fringes also are observed in the HR-TEM images. Different optical properties are observed. The GQDs-G exhibits two absorption bands at 300 nm and 350 nm in the UV-Vis spectrum. There is a relative broad emission band at 445 nm under excitation of 360 nm. The emission band shifts to 510 nm when excitation wavelength changes to 420 nm. The lifetime (Supplementary Figure S10) is not a single exponential decay anymore. It can be fitted as double exponential decay, where $\tau 1$ is 7.9 ns (64.5%) and $\tau 2$ is 1.8 ns (25.5%) (the numbers in
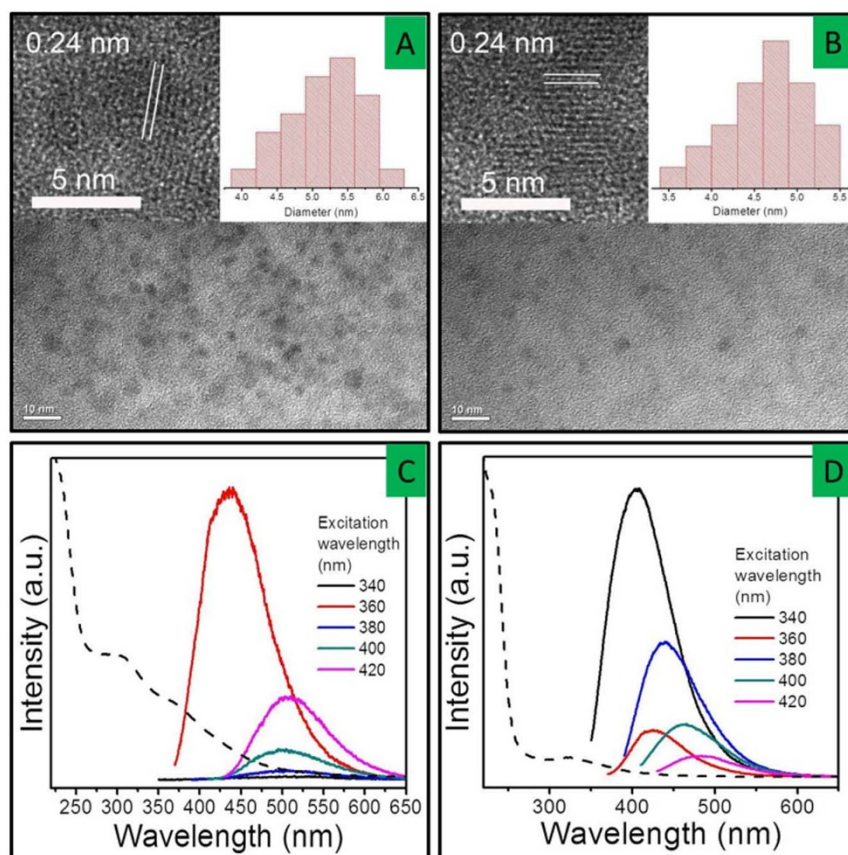

Figure 7 | Characterizations of GQDs-G and GQDs-T. (A) Representative TEM images of GQDs-G. Inset: HR-TEM and particle size distribution. (B) Representative TEM images of GQDs-T. Inset: HR-TEM and particle size distribution. (C) UV-Vis spectra (dash line) and PL spectra (solid lines) of GQDs-G and (D) GQDs-TRIS.

7

parentheses are the percentages of each lifetime). GQDs-TRIS also exhibits an excitation-dependent PL emission and double exponential lifetime decay (τ_{ave} = 6 ns). Both GQDs-G and GQDs-T show relative low PL QY of 6% and 16%, respectively. From above results, citric acid is a better carbon source in the preparation of GQDs through hydrothermal routes.

Discussion

Based on above results and understandings, we believe that the formation of N-doped GQDs involve two steps (Figure 4). At first, the amine works as a base to facilitate the dehydrolysis reaction. CA molecules self-assemble into sheet structure and dehydrolyze to form graphene framework with ~2 nm in diameter[24,32]. During this process, amide molecules are formed between CA and amine. Then the amides react with neighbor carboxylic groups and form pyrrolic N through the second step of intramolecular dehydrolysis. No other type of N state was observed in the XPS, which proves that N atoms enter graphene framework through the intramolecular dehydrolysis between amide and -COOH. Once the pyrrolic N is formed, the PL QY exhibits a significant improvement. Comparing with N free GQDs (GQDs-NaOH), the PL QY of N-doped GQDs increases to 58% for sample GQDs-U-2 with only two hours reaction and trace amount N doped GQDs. GQDs continue to grow with more N doped into the graphene framework along with the reaction. The PL QY of resulting GQDs increases to 78% for GQDs-U-4 sample in which part of N is transferred into graphite N as the reaction undergoing since the ratio of graphite N/pyrrolic N increases. These results are consistent with the C1s XPS results as the relative amount of sp³ C increases with the reaction due to graphite N bonded with C in sp³ form.

Conclusions

We designed and synthesized a series of GQDs in order to investigate the N-doping process through a hydrothermal route. CA was chosen as carbon source because it easily forms graphene framework through intermolecular dehydrolysis. The N enters the graphene framework through intramolecular dehydrolysis and form pyrrolic structure. The pyrrolic N can transform to graphite N in the hydrothermal condition. By changing different types of amine, high PL QY GQDs (94%) can be prepared by using CA as carbon source and EDA as N source. Comparing with other carbon source such as glucose and TRIS, CA is the best precursor for preparation of very high luminescent GQDs.

Methods

Materials. All chemicals are commercial available and analysis pure grade without further purification. Citric acid monohydrate, D-(+)-glucose, tris(hydroxymethyl)aminomethane, NaOH, urea, hexamethylenetetramine, diethylamine, ethanolamine, ethylenediamine were purchased from Beijing Chemicals or Aladdin Chemicals.

Synthesis of GQDs-NaOH. 0.21 g (1 mmol) CA and 0.12 g (3 mmol) NaOH were dissolved into 5 mL water, and stirred to form a clear solution. Then the solution was transferred into a 20 mL Teflon lined stainless autoclave. The sealed autoclave was heated to 160°C in an electric oven and kept for additional 4 hours. The final product was collected by adding ethanol into the solution and centrifuged at 5000 rpm for 5 min. The solid can be easily re-dispersed into water. The obtained samples are denoted as GQDs-xxx, where xxx stands for NaOH or amine abbreviation, for example this sample was denoted as GQDs-NaOH.

Synthesis of N-doped GQDs-U. 0.21 g (1 mmol) CA and 0.18 g (3 mmol) urea were dissolved into 5 mL water, and stirred to form a clear solution. Then the solution was transferred into a 20 mL Teflon lined stainless autoclave. The sealed autoclave was heated to 160°C in an electric oven and kept for additional 4 hours. The final product was collected by adding ethanol into the solution and centrifuged at 5000 rpm for 5 min. The solid can be easily re-dispersed into water.

Synthesis of N-doped GQDs- HMTA. 0.21 g (1 mmol) CA and 0.42 g (3 mmol) HMTA were dissolved into 5 mL water, and stirred to form a clear solution. Then the solution was transferred into a 20 mL Teflon lined stainless autoclave. The sealed autoclave was heated to 160°C in an electric oven and kept for additional 4 hours. The final product was collected by adding ethanol into the solution and centrifuged at 5000 rpm for 5 min. The solid can be easily re-dispersed into water.

Synthesis of N-doped GQDs-EDA. 0.21 g (1 mmol) CA and 0.18 g (3 mmol) EDA were dissolved into 5 mL water, and stirred to form a clear solution. Then the solution was transferred into a 20 mL Teflon lined stainless autoclave. The sealed autoclave was heated to 160°C in an electric oven and kept for additional 4 hours. The final product was collected by adding ethanol into the solution and centrifuged at 5000 rpm for 5 min. The solid can be easily re-dispersed into water.

Synthesis of N-doped GQDs-DEA. 0.21 g (1 mmol) CA and 0.21 g (3 mmol) DEA were dissolved into 5 mL water, and stirred to form a clear solution. Then the solution was transferred into a 20 mL Teflon lined stainless autoclave. The sealed autoclave was heated to 160°C in an electric oven and kept for additional 4 hours. The final product was collected by adding ethanol into the solution and centrifuged at 5000 rpm for 5 min. The solid can be easily re-dispersed into water.

Synthesis of N-doped GQDs-EA. 0.21 g (1 mmol) CA and 0.18 g (3 mmol) EA were dissolved into 5 mL water, and stirred to form a clear solution. Then the solution was transferred into a 20 mL Teflon lined stainless autoclave. The sealed autoclave was heated to 160°C in an electric oven and kept for additional 4 hours. The final product was collected by adding ethanol into the solution and centrifuged at 5000 rpm for 5 min. The solid can be easily re-dispersed into water.

Characterization. Fourier Transform Infrared (FT-IR) spectra of GQDs were recorded as KBr pellets with a Bruker Vertex 70 spectrometer from 4000–500 cm⁻¹. Fluorescence emission spectra were recorded on an LS-55 fluorophotometer. UV-Vis absorption spectra were conducted on a Shimadzu UV-2450 spectrophotometer. HR-TEM images and fast Fourier transform (FFT) spot diagrams were recorded with FEI-TECNAI G2 transmission electron microscope operating at 200 kV. X-Ray photoelectron spectra were obtained on a Thermo Scientific ESCALAB 250 Multitechnique Surface Analysis with Al Kα X-ray monochromator, pass energy 20 eV. Raman spectra were recorded on Jobin Yvon Horiba LAB-RAM Infinity with 325 nm laser beam. Absolute quantum yield were obtained in a calibrated integrating sphere on Edinburgh FLS920 spectrometer. Lifetime experiments were obtained on Edinburgh TSCPS FL 920. Atomic Force Microscope (AFM) images were recorded with Bruker multi-mode 8.

1. Ritter, K. A. & Lyding, J. W. The Influence of Edge Structure on the Electronic Properties of Graphene Quantum Dots and Nanoribbons. *Nat. Mater.* **8**, 235–242 (2009).
2. Baker, S. N. & Baker, G. A. Luminescent Carbon Nanodots: Emergent Nanolights. *Angew. Chem. Int. Ed.* **49**, 6726–6744 (2010).
3. Shen, J., Zhu, Y., Yang, X. & Li, C. Graphene Quantum Dots: Emergent Nanolights for Bioimaging, Sensors, Catalysis and Photovoltaic Devices. *Chem. Commun.* **48**, 3686–3699 (2012).
4. Li, L.-S. & Yan, X. Colloidal Graphene Quantum Dots. *J. Phys. Chem. Lett.* **1**, 2572–2576 (2010).
5. Li, L., Wu, G., Yang, G., Peng, J., Zhao, J. & Zhu, J.-J. Focusing on Luminescent Graphene Quantum Dots: Current Status and Future Perspectives. *Nanoscale* **5**, 4015–4039 (2013).
6. Cao, L., Meziani, M. J., Sahu, S. & Sun, Y.-P. Photoluminescence Properties of Graphene versus Other Carbon Nanomaterials. *Acc. Chem. Res.* **46**, 171–180 (2012).
7. Li, H. *et al.* Water-Soluble Fluorescent Carbon Quantum Dots and Photocatalyst Design. *Angew. Chem. Int. Ed.* **49**, 4430–4434 (2010).
8. Yan, X., Cui, X., Li, B. & Li, L.-S. Large, Solution-Processable Graphene Quantum Dots as Light Absorbers for Photovoltaics. *Nano Lett.* **10**, 1869–1873 (2010).
9. Jin, S. H., Kim, D. H., Jun, G. H., Hong, S. H. & Jeon, S. Tuning the Photoluminescence of Graphene Quantum Dots through the Charge Transfer Effect of Functional Groups. *ACS Nano* **7**, 1239–1245 (2012).
10. Gupta, V., Chaudhary, N., Srivastava, R., Sharma, G. D., Bhardwaj, R. & Chand, S. Luminscent Graphene Quantum Dots for Organic Photovoltaic Devices. *J. Am. Chem. Soc.* **133**, 9960–9963 (2011).
11. Zhu, S. *et al.* Strongly Green-Photoluminescent Graphene Quantum Dots for Bioimaging Applications. *Chem. Commun.* **47**, 6858–6860 (2011).
12. Liu, R., Wu, D., Feng, X. & Muellen, K. Bottom-Up Fabrication of Photoluminescent Graphene Quantum Dots with Uniform Morphology. *J. Am. Chem. Soc.* **133**, 15221–15223 (2011).
13. Li, Y. *et al.* An Electrochemical Avenue to Green-Luminescent Graphene Quantum Dots as Potential Electron-Acceptors for Photovoltaics. *Adv. Mater.* **23**, 776–780 (2011).
14. Wang, Y., Shao, Y., Matson, D. W., Li, J. & Lin, Y. Nitrogen-Doped Graphene and Its Application in Electrochemical Biosensing. *ACS Nano* **4**, 1790–1798 (2010).
15. Cao, L. *et al.* Carbon Nanoparticles as Visible-Light Photocatalysts for Efficient CO2 Conversion and Beyond. *J. Am. Chem. Soc.* **133**, 4754–4757 (2011).
16. Ding, C., Zhu, A. & Tian, Y. Functional Surface Engineering of C-Dots for Fluorescent Biosensing and in Vivo Bioimaging. *Acc. Chem. Res.* **47**, 20–30 (2014).
17. Zheng, M. *et al.* Integrating Oxaliplatin with Highly Luminescent Carbon Dots: An Unprecedented Theranostic Agent for Personalized Medicine. *Adv. Mater.* **26**, DOI: 10.1002/adma.201306192 (2014).
18. Peng, J. *et al.* Graphene Quantum Dots Derived from Carbon Fibers. *Nano Lett.* **12**, 844–849 (2012).

19. Zhu, S. *et al.* Highly Photoluminescent Carbon Dots for Multicolor Patterning, Sensors, and Bioimaging. *Angew. Chem. Int. Ed.* **52**, 3953–3957 (2013).
20. Pan, D., Zhang, J., Li, Z. & Wu, M. Hydrothermal Route for Cutting Graphene Sheets into Blue-Luminescent Graphene Quantum Dots. *Adv. Mater.* **22**, 734–738 (2010).
21. Yan, X., Cui, X. & Li, L.-S. Synthesis of Large, Stable Colloidal Graphene Quantum Dots with Tunable Size. *J. Am. Chem. Soc.* **132**, 5944–5945 (2010).
22. Lu, J., Yeo, P. S. E., Gan, C. K., Wu, P. & Loh, K. P. Transforming C60 Molecules into Graphene Quantum Dots. *Nat. Nano.* **6**, 247–252 (2011).
23. Tang, L. *et al.* Deep Ultraviolet Photoluminescence of Water-Soluble Self-Passivated Graphene Quantum Dots. *ACS Nano* **6**, 5102–5110 (2012).
24. Dong, Y. *et al.* Blue Luminescent Graphene Quantum Dots and Graphene Oxide Prepared by Tuning the Carbonization Degree of Citric Acid. *Carbon* **50**, 4738–4743 (2012).
25. Dong, Y. *et al.* Carbon-Based Dots Co-doped with Nitrogen and Sulfur for High Quantum Yield and Excitation-Independent Emission. *Angew. Chem. Int. Ed.* **52**, 7800–7804 (2013).
26. Li, Y. *et al.* Nitrogen-Doped Graphene Quantum Dots with Oxygen-Rich Functional Groups. *J. Am. Chem. Soc.* **134**, 15–18 (2012).
27. Qu, S., Wang, X., Lu, Q., Liu, X. & Wang, L. A Biocompatible Fluorescent Ink Based on Water-Soluble Luminescent Carbon Nanodots. *Angew. Chem. Int. Ed.* **51**, 12215–12218 (2012).
28. Li, X., Zhang, S., Kulinich, S. A., Liu, Y. & Zeng, H. Engineering surface states of carbon dots to achieve controllable luminescence for solid-luminescent composites and sensitive Be2+ detection. *Sci. Rep.* **4**, 4976 (2014).
29. Du, F., Zeng, F., Ming, Y. & Wu, S. Carbon Dots-Based Fluorescent Probes for Sensitive and Selective Detection of Iodide. *Microchim. Acta* **180**, 453–460 (2013).
30. Wang, F., Pang, S., Wang, L., Li, Q., Kreiter, M. & Liu, C.-Y. One-Step Synthesis of Highly Luminescent Carbon Dots in Noncoordinating Solvents. *Chem. Mater.* **22**, 4528–4530 (2010).
31. Zhu, S. *et al.* Surface Chemistry Routes to Modulate the Photoluminescence of Graphene Quantum Dots: From Fluorescence Mechanism to Up-Conversion Bioimaging Applications. *Adv. Funct. Mater.* **22**, 4732–4740 (2012).
32. Qu, D. *et al.* Highly Luminescent S, N Co-doped Graphene Quantum Dots with Broad Visible Absorption Bands for Visible Light Photocatalysts. *Nanoscale* **5**, 12272–12277 (2013).
33. Ding, W. *et al.* Space-Confinement-Induced Synthesis of Pyridinic- and Pyrrolic-Nitrogen-Doped Graphene for the Catalysis of Oxygen Reduction. *Angew. Chem. Int. Ed.* **52**, 11755–11759 (2013).
34. Cushing, S. K., Li, M., Huang, F. & Wu, N. Origin of Strong Excitation Wavelength Dependent Fluorescence of Graphene Oxide. *ACS Nano* **8**, 1002–1013 (2013).

Acknowledgments

Author contributions

D.Q., M.Z. and Z.S. design and study of experiments and research. L.Z. and H.Z. contributed to the electron microscopy results, Z.X. and X.J. contributed to the lifetime of GQDs. R.H. and H.F. contributed to the discussion of all the data. All authors reviewed the manuscript.

Additional information

Supplementary information accompanies this paper at http://www.nature.com/scientificreports

Competing financial interests: The authors declare no competing financial interests.

How to cite this article: Qu, D. *et al.* Formation mechanism and optimization of highly luminescent N-doped graphene quantum dots. *Sci. Rep.* **4**, 5294; DOI:10.1038/srep05294 (2014).

CORRIGENDUM: Formation mechanism and optimization of highly luminescent N-doped graphene quantum dots

Dan Qu, Min Zheng, Ligong Zhang, Haifeng Zhao, Zhigang Xie, Xiabin Jing, Raid E. Haddad, Hongyou Fan & Zaicheng Sun

This Article contains an error in figure 5. Data from figure 1b is duplicated in figure 5e. The correct figure 5 appears below as figure 1.

Figure 1 |